Gastroenterology 2021;160:797–808

# Epithelial TLR4 Signaling Activates DUOX2 to Induce Microbiota-Driven Tumorigenesis

Juan F. Burgueño,[1] Julia Fritsch,[1,2] Eddy E. González,[3] Kevin S. Landau,[1] Ana M. Santander,[1] Irina Fernández,[1] Hajar Hazime,[1] Julie M. Davies,[1] Rebeca Santaolalla,[1] Matthew C. Phillips,[1] Sophia Diaz,[1] Rishu Dheer,[1] Nivis Brito,[1] Judith Pignac-Kobinger,[1] Ester Fernández,[4] Gregory E. Conner,[5] and Maria T. Abreu[1,2]

*[1]Department of Medicine, Division of Gastroenterology, University of Miami–Miller School of Medicine, Miami, Florida; [2]Department of Microbiology and Immunology, University of Miami–Miller School of Medicine, Miami, Florida; [3]Biotechnology and Biopharmaceuticals Laboratory, Department of Pathophysiology, School of Biological Science, Universidad de Concepción, Concepción, Chile; [4]Animal Physiology Unit, Department of Cell Biology, Physiology and Immunology, Universitat Autònoma de Barcelona, Barcelona, Spain; and [5]Department of Cell Biology, University of Miami–Miller School of Medicine, Miami, Florida*

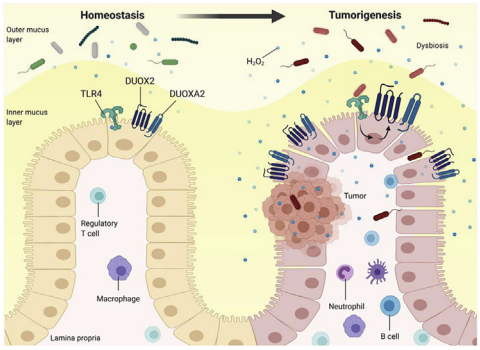


**BACKGROUND & AIMS:** Chronic colonic inflammation leads to dysplasia and cancer in patients with inflammatory bowel disease. We have described the critical role of innate immune signaling via Toll-like receptor 4 (TLR4) in the pathogenesis of dysplasia and cancer. In the current study, we interrogate the intersection of TLR4 signaling, epithelial redox activity, and the microbiota in colitis-associated neoplasia. **METHODS:** Inflammatory bowel disease and colorectal cancer data sets were analyzed for expression of TLR4, dual oxidase 2 (DUOX2), and NADPH oxidase 1 (NOX1). Epithelial production of hydrogen peroxide ($H_2O_2$) was analyzed in murine colonic epithelial cells and colonoid cultures. Colorectal cancer models were carried out in villin-TLR4 mice, carrying a constitutively active form of TLR4, their littermates, and villin-TLR4 mice backcrossed to DUOXA-knockout mice. The role of the TLR4-shaped microbiota in tumor development was tested in wild-type germ-free mice. **RESULTS:** Activation of epithelial TLR4 was associated with up-regulation of *DUOX2* and *NOX1* in inflammatory bowel disease and colorectal cancer. DUOX2 was exquisitely dependent on TLR4 signaling and mediated the production of epithelial $H_2O_2$. Epithelial $H_2O_2$ was significantly increased in villin-TLR4 mice; TLR4-dependent tumorigenesis required the presence of DUOX2 and a microbiota. Mucosa-associated microbiota transferred from villin-TLR4 mice to wild-type germ-free mice caused increased $H_2O_2$ production and tumorigenesis. **CONCLUSIONS:** Increased TLR4 signaling in colitis drives expression of DUOX2 and epithelial production of $H_2O_2$. The local milieu imprints the mucosal microbiota and imbues it with pathogenic properties demonstrated by enhanced epithelial reactive oxygen species and increased development of colitis-associated tumors. The interrelationship between epithelial reactive oxygen species and tumor-promoting microbiota requires a 2-pronged strategy to reduce the risk of dysplasia in colitis patients.

*Keywords:* Ulcerative Colitis; NADPH Oxidases; Colitis-Associated Cancer; Microbiome.

Inflammatory bowel diseases (IBDs) are common and are increasing in incidence as more parts of the world are becoming industrialized.[1] Patients with long-standing ulcerative colitis (UC) are at increased risk of developing colorectal cancer (CRC) compared with the general population.[2] As prevalence of IBD increases, this raises concern

***Abbreviations used in this paper:*** **AIEC, adherent invasive *Escherichia coli*; AOM, azoxymethane; CAC, colitis-associated cancer; CEC, colonic epithelial cell; CRC, colorectal cancer; DSS, dextran sulfate sodium; DPI, diphenyleneiodonium; DUOX2, dual oxidase 2; DUOXA2, dual oxidase maturation factor 2; GF, germ-free; $H_2O_2$, hydrogen peroxide; IBD, inflammatory bowel disease; KO, knockout; LPS, lipopolysaccharide; NOX1, NADPH oxidase 1; NOXA1, Nox activator 1; NOXO1, Nox organizer 1; PCR, polymerase chain reaction; ROS, reactive oxygen species; SPF, specific pathogen-free; TLR4, Toll-like receptor 4; UC, ulcerative colitis.**

**Most current article**


0016-5085/$36.00
https://doi.org/10.1053/j.gastro.2020.10.031

**WHAT YOU NEED TO KNOW**

BACKGROUND AND CONTEXT

Epithelial NADPH oxidase DUOX2 is up-regulated in biopsies from patients with IBD and colorectal cancer but the functional implications are unknown.

NEW FINDINGS

The microbiota activate TLR4 which in turn stimulates epithelial ROS through DUOX2. Increased epithelial ROS production is associated with pro-tumorigenic microbiota. Both an altered microbiota and epithelial ROS are needed for colonic tumorigenesis.

LIMITATIONS

Our experiments require corroboration in IBD patients.

IMPACT

Our data show that microbial-induced epithelial ROS participate in tumorigenesis even in the absence of overt inflammation, shedding light on why certain patients develop dysplasia long after the active inflammation has been treated.

for an increase in worldwide cases of colitis-associated CRC (CAC).[3,4] The intensity, extent, and duration of inflammation all contribute to an increased risk of cancer.[5] The most recent population-based studies estimate that 15%–20% of IBD patients with pancolitis develop CAC after 10 years of disease.[3,4] CAC has a poorer survival rate than sporadic CRC in advanced and metastatic stages, and accounts for 15% of the mortality in IBD patients.[6,7] Yet, progression from dysplasia to cancer is poorly understood.

Two hallmarks of IBD and CAC are the abnormal host response towards the microbiota[8,9] and the alterations in the microbial composition, termed *dysbiosis*.[10,11] In humans, it is difficult to tease out whether inflammation or dysbiosis comes first.[12] One host-dependent mechanism proposed to induce alterations in the microbiota at a compositional and functional level is the production of reactive oxygen species (ROS).[13,14] Whereas ROS production during inflammation has been attributed largely to infiltrating immune cells, the release of reactive oxygen intermediates by the epithelium has not been explored thoroughly. Epithelial ROS are produced as byproducts of mitochondrial activity or via NADPH oxidases, which are essential for the protection of the host against microbial tissue colonization.[14–16] Indeed, mutations in the NADPH oxidase dual oxidase 2 (DUOX2) have been associated with increased pathogen invasiveness and development of IBD[17] and very-early-onset IBD.[18,19] However, a characteristic of IBD is recapitulation of an immune response against commensal microbes in the absence of a known pathogen. In established UC, the mucosa is characterized by an up-regulation in DUOX2.[11,20] We and others have demonstrated that this enzyme is induced by microbial stimuli[21,22] and drives epithelial hydrogen peroxide ($H_2O_2$) release in response to interferon gamma and flagellin.[22] However, the consequences of DUOX2 overexpression during inflammation have not been investigated.

Given the link between inflammation, CAC, and the microbiota, we have been interested in the contribution of innate immune responses in the progression from inflammation to CAC. Toll-like receptor 4 (TLR4) is an innate immune receptor that recognizes Gram-negative lipopolysaccharide (LPS), triggering antimicrobial and proinflammatory responses.[23,24] We have reported the overexpression of TLR4 in the colonic epithelial cells (CECs) of patients with UC and CRC.[25,26] Transgenic mice expressing a constitutively active TLR4 in the intestinal epithelium, villin-TLR4, are more susceptible to inflammation, CRC, and CAC, and have a mucosal microbiome that is shaped by TLR4 signaling.[27,28] Notably, the microbiota of villin-TLR4 mice can transmit susceptibility to colitis in wild-type mice.[27]

In the current study, we interrogate the interplay among up-regulated epithelial TLR4 signaling, the microbiota, and the development of tumorigenesis. In an unbiased search for genes regulated by TLR4 in the setting of CAC, the most highly expressed genes are involved in ROS generation by CECs. We demonstrate that epithelial TLR4 drives the expression of DUOX2 and the production of $H_2O_2$ by CECs. We also show that TLR4-shaped microbiota and DUOX2 participate in tumor initiation and that TLR4-shaped microbiota, which induces epithelial ROS production, is sufficient to transmit susceptibility to CAC. We believe that our study sheds light on a mechanism through which innate immune responses to the microbiota, even in the absence of overt inflammation, accelerate the transition from inflammation to dysplasia in IBD. This situation mimics what is observed in patients whose colitis is controlled but progresses to dysplasia and cancer.

## Methods

### Animals

Villin-TLR4 mice expressing the CD4-TLR4 transgene[23] under the villin promoter were generated as described previously.[29] TLR4 knock-out (TLR4-KO; 10ScNJ), NOX1-KO ($Nox1^{tm1Kkr}$), and C57Bl/6 mice were purchased from the Jackson Laboratory. Epithelial DUOXA1/A2-KO mice (DUOXA-KO) were obtained by crossing the D*uoxA1/A2*-floxed mice generated at Dr Kaunitz's laboratory (University of California, Los Angeles) with villin-cre (Tg(Vil1-cre)997Gum) mice purchased from the Jackson Laboratory. These mice are widely accepted as a model to investigate the role of DUOX2 in the colon, given that the expression of DUOX1 in the gut is exceedingly low.[21] Villin-TLR4 DUOXA-KO mice were generated by backcrossing both strains. All mice, generated on a C57Bl/6 background, were housed in specific pathogen-free (SPF) conditions with a controlled temperature of 20°C ± 2°C and free access to food and water. All experiments were performed using mice between 8 and 16 weeks of age, of both sexes, with the approval of the Institutional Animal Care and Use Committee at the University of Miami (Protocols 17-196 and 18-169). The University of Miami is

internationally accredited by the Association for Assessment and Accreditation of Laboratory Animal Care.

### Germ-Free Mice and Microbial Engraftment

Wild-type and villin-TLR4 germ-free (GF) mice were generated at the University of Miami Gnotobiotic Facility. Microbial engraftment was performed by transferring the mucosa-associated microbiota from C57Bl/6J or villin-TLR4 donor mice to wild-type GF recipient mice. Briefly, the mucosa-associated microbiota was extracted by homogenizing flushed colons in Hank's balanced salt solution using a BeadBlaster-24 (Benchmark) in a vinyl anaerobic chamber (Coy Laboratory Products). One milliliter of Hank's balanced salt solution was used for every 50 mg of colon. Wild-type GF recipient mice were orally gavaged with 200 $\mu$L of the resulting slurry and housed in separate biocontainment unit isocages, depending on the donor mouse microbiome (vilin-TLR4 vs C57Bl/6J). After 3 weeks of engraftment, 2 recipient mice per each donor mouse were euthanized and a piece of mucosa was analyzed by 16s ribosomal RNA sequencing to verify engraftment. The remaining mice underwent the azoxymethane/dextran sulfate sodium (AOM-DSS) model of tumorigenesis.

### Induction of Tumorigenesis

To investigate tumorigenesis, the following 2 models were utilized: the AOM-DSS model of CAC and the AOM model of CRC. In the AOM-DSS model, mice were injected intraperitoneally once with 7.4 mg/kg AOM (Sigma-Aldrich) and then administered 2 or 3 cycles of DSS (Affymetrix USB, molecular weight 40,000–50,000) in their drinking water for 5–7 consecutive days, depending on the experiment. Because villin-TLR4 mice are more susceptible to DSS,[28] they were treated with 1.5% DSS, while engrafted mice and wild-type littermates received 3% DSS. To analyze the various stages of tumor development, mice were euthanized on day 35 (dysplastic phase), 56, or 72 (tumor phases). During the DSS cycles and the first recovery week mice were monitored daily for weight loss. Fluid supplementation was applied to mice losing >25% of their initial body weight,[30] whereas end-point criteria were applied to mice losing >30% of their initial body weight or displaying lack of exploratory behavior.

In the AOM model of CRC, mice were injected intraperitoneally with 14.8 mg/kg AOM once a week for 6 consecutive weeks and were euthanized at weeks 12 or 17, as described previously.[25] GF status at the end of the experiment was corroborated by 16s ribosomal RNA polymerase chain reaction (PCR) from stool collected directly from the colon during euthanasia (Supplementary Figure 4).

### Collection of Tissue Samples

Mice were euthanized by cervical dislocation under isoflurane (Piramal Critical Care) anesthesia and the colon was removed, flushed, cut wide open, and pinned flat on a Sylgard-coated Petri dish. Tumor lesions imaged under a Nikon SMZ800 stereomicroscope were stitched using Adobe Photoshop CC (Adobe Systems Inc) and quantified for number and size using ImageJ software (National Institutes of Health). A longitudinal section of the colon was prepared as a Swiss roll and fixed in 4% paraformaldehyde for histology, and the rest of the colon was used for CEC isolation. Tumor surrounding areas were homogenized in TRIzol reagent (ThermoFisher Scientific) for RNA isolation.

### Isolation of Colonic Epithelial Cells and Colonoid Preparation

CECs were isolated by chelation in 20 mM EDTA in Hank's balanced salt solution for 1 hour at room temperature, followed by gentle shaking. CECs were either lysed in TRIzol reagent for quantitative PCR or pelleted for determination of $H_2O_2$ production and preparation of colonoids. Before seeding the colonoids, the crypts were digested with Dispase (StemCell Technologies; 1 U/L) in the presence of 2.5 $\mu$M Thiazovivin (Cayman Chemical) to obtain single-cell suspension, and then resuspended in ice-cold Cultrex reduced growth factor basement membrane, type R1 (R&D Systems). Colonoids were initially grown in 50% conditioned medium containing wnt3a, R-spondin-3, noggin, and 20% fetal bovine serum supplemented with glycogen synthase kinase 3$\beta$ inhibitor Chir99021 (5 $\mu$M), 2.5 $\mu$M Thiazovivin, and 100 $\mu$g/mL Primocin. After 2 days of expansion, colonoids were cultured for an additional 5 days in medium containing Dulbecco's modified Eagle medium/F12, 10% R-spondin-2 and 10% noggin-conditioned media, 10% fetal bovine serum, Primocin, and Chir00921. Colonoids were challenged with ultrapure LPS (1 $\mu$g/mL), interferon gamma (100 ng/mL), heat-killed *Faecalibacterium prausnitzii* ($10^6$ cells/mL, strain A2-165), or adherent invasive *Escherichia coli* (AIEC; $10^6$ cells/mL, AIEC strain LF82) for 24 hours before determinations.

### Measurement of Hydrogen Peroxide Production

Amplex red (ThermoFisher Scientific) was used to measure the real-time kinetics of $H_2O_2$ production by live cells. CECs or colon organoids seeded in a 96-well plate were incubated in Dulbecco's phosphate-buffered saline solution containing $Ca^{2+}$, $Mg^{2+}$, 0.1 U/mL horseradish peroxidase, and 30 $\mu$M Amplex red (per manufacturer's instructions) with modifications.[22] Dimethyl sulfoxide (vehicle) or 10 $\mu$M of the NADPH oxidase inhibitor diphenyleneiodonium (DPI) were added to assess $H_2O_2$ production induced by NADPH oxidases. Fluorescence was read at 40- to 60-second intervals for 10 minutes at 37°C (Ex 530 nm/Em 590 nm) in a Synergy H1 fluorometer (Bio-Tek). $H_2O_2$ production was normalized to cell viability via MTT assay (ATCC) that was performed per manufacturer's instructions. All samples were assayed in triplicate.

### Statistical Analysis

All data analysis and plots were performed using Prism8 (GraphPad Software) and compared using chi-square, $t$ test, or 2-way analysis of variance, as indicated. Results are presented as mean values and SD, and a $P$ value of $<.05$ was considered significant.

## Results

### Dysregulation of Toll-Like Receptor 4 Is Associated With Overexpression of DUOX2 and NOX1

We have previously reported that UC patients with dysplasia have increased intestinal epithelial expression of

TLR4[31] and that activation of TLR4 in CECs renders mice more susceptible to tumorigenesis.[25,28] To take an unbiased view of the molecular signature of TLR4-dependent tumorigenesis, we used gene expression arrays (Mouse Exonic Evidence-Based Oligonucleotide microarray) to look for differentially expressed genes. Villin-TLR4 mice or wild-type littermate controls were treated with AOM-DSS[28] and tissue from areas surrounding tumors was collected to analyze the gene expression changes in nondysplastic at-risk epithelium. Several pathways related to immune activation were up-regulated in villin-TLR4 mice compared with their littermates (Supplementary Material; GSE141767). Enzymes associated with ROS production, including inducible nitric oxide synthase (*Nos2*), *Duox2*, and *Nox1*, were among the most differentially up-regulated genes in villin-TLR4 mucosa (Figure 1*A*).

The role of the NADPH oxidases DUOX2 and NOX1 in IBD or CAC is poorly understood. To identify how TLR4 expression correlates with expression of NADPH oxidases in human disease, we used a bioinformatics approach. We interrogated available gene expression datasets of Crohn's disease, UC (GSE10616[32]), and CRC patients (GSE8671[33]) for the expression of *TLR4*, *DUOX2*, and *NOX1*. We found that *TLR4* and *DUOX2* transcripts were significantly increased in UC, whereas *TLR4*, *DUOX2*, and *NOX1* were all up-regulated in Crohn's disease and CRC patients (Figure 1*B* and *C*, Supplementary Figure 1*A* and *B*; *left panels*). Furthermore, we generated gene set enrichment analysis plots for these data sets for pathways related to ROS metabolism stratified by TLR4 expression and observed that *DUOX2*, but not *NOX1*, was consistently found in the leading-edge genes associated with increased expression of TLR4 (Figure 1*B* and *C*, Supplementary Figure 1*A* and *B*; *right panels*). These data suggest that the NADPH oxidases DUOX2 and NOX1 are linked to TLR4 up-regulation in UC, Crohn's disease, and CRC samples, as well as in our TLR4-dependent murine model of CAC.

## Bacterial Signaling Through Toll-Like Receptor 4 Regulates Expression of Duox2 and Nox1 in Colonic Epithelial Cells In Vivo and In Vitro

Our data in a murine model of TLR4-dependent CAC and patients with UC or CRC suggest that DUOX2 and NOX1 are regulated by TLR4. We next wished to determine whether TLR4 and the microbiota regulate *Duox2* and *Nox1* in CECs. To address this question, we used CECs or colon tissues from villin-TLR4 and wild-type littermates raised in SPF vs GF conditions. We compared messenger RNA expression of *Duox2* and *Nox1* by in situ hybridization and quantitative PCR, and their respective regulator proteins *Duoxa2*, *Noxo1*, *Noxa1*, and *Cyba*[34,35] by quantitative PCR. We found that wild-type GF mice had reduced expression of *Duox2* and *Duoxa2* compared with wild-type SPF mice (Supplementary Figure 2*B*). Consistently, *Duox2* transcripts in wild-type GF mice were clearly reduced and expressed at the bottom of the crypt compared with SPF mice, which essentially expressed *Duox2* at the tips of the crypts (Figure 2*A*). Constitutive activation of TLR4 in villin-TLR4 mice induced the expression of NADPH oxidases in SPF mice and restored expression of these genes under GF conditions (Figure 2*B*). *Duox2* was induced all along the crypt axis and more markedly at the tips of the crypts, whereas *Nox1* transcripts accumulated at the lower one-third of the crypt (Figure 2*A* and Supplementary Figure 2*A*). Only *Noxo1* was TLR4-independent, as indicated by 2-way analysis of variance ($P < .05$ in *Noxa1* and $P < .001$ in *Duox2*, *Duoxa2*, *Nox1*, and *Cyba* transcripts). These data demonstrate that *Duox2* and *Nox1* are regulated by the microbiota and that TLR4 signaling is sufficient to induce their expression.

To further investigate whether *Duox2* and *Nox1* expression depends strictly on TLR4, we isolated CECs from TLR4-KO and wild-type mice raised in SPF conditions and compared the gene expression for *Duox2*, *Nox1*, and related genes. Steady-state levels of *Duox2* and *Duoxa2*, but not NOX1-associated genes, were highly dependent on TLR4, as TLR4-KO CECs had significantly reduced transcript levels for both genes (Figure 2*C* and Supplementary Figure 2*C*). These results indicate that DUOX2 is tightly regulated by TLR4, whereas redundant mechanisms control expression of NOX1.

To corroborate that TLR4-mediated induction of NADPH oxidase expression occurs primarily in CECs and is not dependent on interactions with other cell types, we cultured wild-type and TLR4-KO colonoids and stimulated them with LPS for 24 hours. In contrast to TLR4-KO cells, wild-type colonoids up-regulated *Duox2*, *Duoxa2*, and *Nox1* on stimulation with LPS, corroborating that epithelial TLR4 activation is sufficient to up-regulate *Duox2* and *Nox1* in CECs (Figure 2*D* and Supplementary Figure 2*D*). Furthermore, we tested the requirement of TLR4 to respond to IBD-relevant bacteria, namely *F prausnitzii* and AIEC. *F prausnitzii* is a Gram-positive bacteria with a recognized protective role in IBD,[36] whereas AIEC is a Gram-negative pathobiont often associated with development and aggravation of IBD.[37] Interestingly, while heat-killed *F prausnitzii* did not induce the up-regulation of NADPH oxidases, AIEC induced expression of *Duox2*, *Duoxa2*, *Nox1*, and *Cyba* in a TLR4-dependent manner (Figure 2*E* and Supplementary Figure 2*E*). These results suggest that CECs up-regulate expression of NADPH oxidases in response to bacterial recognition via TLR4, and that DUOX2 is highly dependent on TLR4 signaling.

## Epithelial Toll-Like Receptor 4 Activation Induces $H_2O_2$ Production in a DUOX2-Dependent Manner

We next sought to determine the functional correlate of TLR4-induced NADPH oxidase expression, namely production of $H_2O_2$. To measure epithelial $H_2O_2$ production, we recently described a modified Amplex Red assay that can be used in CECs.[22] Freshly isolated CECs from villin-TLR4 mice had a marked increase in the production rate of $H_2O_2$ compared with wild-type CECs (Figure 3*A*). Furthermore, while CECs isolated from wild-type GF mice produced less $H_2O_2$ than those isolated from wild-type SPF mice (Supplementary Figure 3*A*), constitutively active TLR4 in villin-TLR4 GF mice sustained high levels of $H_2O_2$ production, demonstrating that TLR4 signaling is sufficient to induce epithelial release of $H_2O_2$ (Figure 3*A*). Wild-type and TLR4-KO CECs showed similar rates of steady-state $H_2O_2$

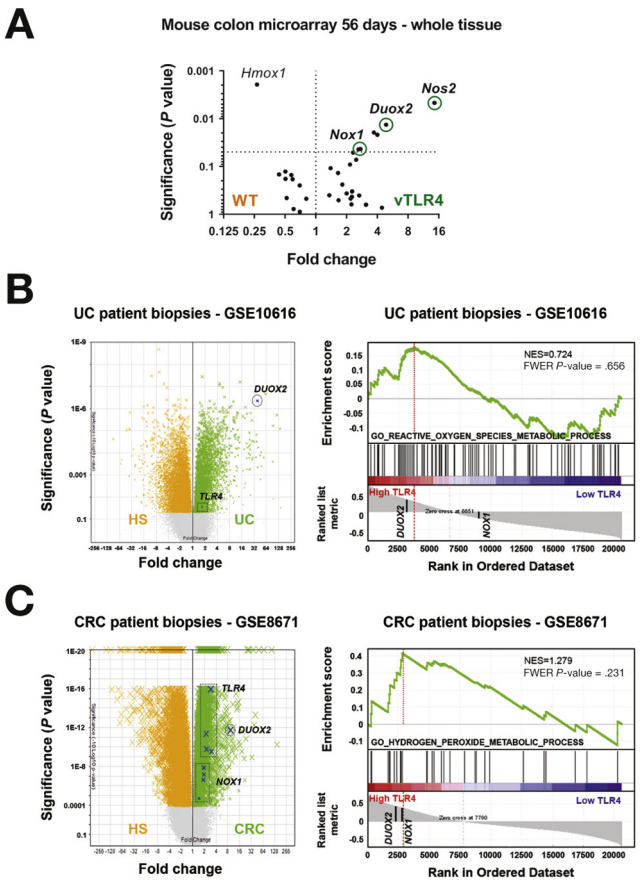


**Figure 1.** Activation of TLR4 is associated with up-regulation of NADPH oxidases in colonic tissue. (*A*) Noninvolved areas surrounding tumors were assayed on a microarray. *Volcano plot* shows the most representative up-regulated genes in villin-TLR4 (vTLR4) mice and their wild-type (WT) littermates for ROS-associated pathways. (*B*) Expression of *TLR4*, *DUOX2*, and *NOX1* in the data set GSE10616 of UC patient biopsies. *Volcano plot* shows *TLR4* and *DUOX2* in UC patients vs healthy subjects (HS). *Boxes* highlight the location of different probes for the same transcript. Gene set enrichment analysis (GSEA) plot shows that *DUOX2* is in the leading-edge genes up-regulated in association with *TLR4* overexpression. (*C*) Expression of *TLR4*, *DUOX2*, and *NOX1* in the data set GSE8671 of CRC patient biopsies. *Volcano plot* shows gene expression in CRC adenoma vs healthy tissue. GSEA plot shows that *DUOX2* and *NOX1* are in the leading-edge genes up-regulated in association with *TLR4* overexpression.

production in SPF conditions (Supplementary Figure 3*B*). To determine the involvement of NADPH oxidases in TLR4-induced epithelial $H_2O_2$ production, freshly isolated CECs were assayed for $H_2O_2$ production and treated with the NADPH oxidase inhibitor DPI or vehicle (dimethyl sulfoxide). DPI significantly reduced the production rates of $H_2O_2$ in both wild-type and villin-TLR4 CECs compared with dimethyl sulfoxide (Figure 3*B*). Similarly, wild-type colonoids stimulated with LPS for 24 hours showed an increased release of $H_2O_2$ that was blocked by incubation with DPI (Figure 3*C*). These experiments demonstrate that TLR4-mediated $H_2O_2$ production is dependent on NADPH oxidase activity. Specificity of TLR4 activation by LPS was confirmed in TLR4-KO colonoids, which did not respond to LPS challenge (Figure 3*C*), but did respond to stimulation with interferon gamma (Supplementary Figure 3*C*).

Next, to assess the relative contribution of DUOX2 and NOX1 to $H_2O_2$ production downstream of TLR4, we generated colonoids from DUOXA-KO and NOX1-KO mice. In the absence of NOX1, LPS-induced $H_2O_2$ production was not reduced compared with wild-type colonoids (Figure 3*D*). Conversely, absence of DUOXA resulted in a total lack of response to LPS compared with that of their control colonoids (DUOXA-wild-type floxed organoids not expressing the villin-cre recombinase) (Figure 3*D*). These data suggest that DUOX2 is the main NADPH oxidase involved in TLR4-dependent induction of $H_2O_2$. Finally, we investigated the requirement for TLR4, NOX1, and DUOX2 to produce epithelial $H_2O_2$ in response to IBD-relevant bacteria. Although stimulation with heat-killed *F prausnitzii* did not induce release of $H_2O_2$, AIEC caused a marked increase in the production of epithelial ROS that was abrogated in TLR4, NOX1, and DUOXA-KO colonoids (Figure 3*E*). These observations indicate that CECs respond to Gram-negative bacterial challenge by inducing NADPH oxidase-mediated release of ROS in a TLR4-dependent fashion.

## *Colitis-Associated Dysplasia and Tumorigenesis Are Associated With Increased $H_2O_2$ Synthesis by Colonic Epithelial Cells*

We have shown that villin-TLR4 mice develop more and larger tumors when challenged with AOM-DSS.[28] We showed that NADPH oxidase–mediated production of $H_2O_2$ is elevated in CECs from villin-TLR4 mice. To examine the dynamic production of $H_2O_2$ by CECs and the relationship to dysplasia and tumor development in wild-type vs villin-TLR4 mice, we performed the AOM-DSS model. To look at the relationship of epithelial $H_2O_2$ production to the inflammation–dysplasia cascade, we euthanized mice during the second cycle of DSS, before tumor development, or 2 weeks after the second cycle, when tumors are established (Figure 4*A*). Our results showed that administration of 1.5% DSS in villin-TLR4 mice and 3% DSS in their wild-type littermates led to the development of high-grade dysplasia in 100% of villin-TLR4 mice, whereas only 43% of wild-type littermates developed any degree of dysplasia (3 of 7 wild-type vs 7 of 7 villin-TLR4 mice; $P < .05$; Figure 4*B*). By day 56, villin-TLR4 mice had extensive tumor development compared with wild-type mice (Figure 4*C*). Villin-TLR4 mice lesions were characterized by marked nuclear crowding, with stratification and hyperchromasia, as well as the presence of cribriform patterns reminiscent of that seen in patients with high-grade dysplasia (Figure 4*D*). In contrast, wild-type littermates showed a higher proportion of regenerative crypts, with clear differentiation towards the epithelial surface, as well as a lower inflammation score (Figure 4*D*). Coincident with this, we observed increased production of CEC $H_2O_2$ after subsequent DSS challenges, which was significantly higher in villin-TLR4 mice CECs compared with those of wild-type littermates (Figure 4*E*). Two-way analysis of variance identified an interaction effect

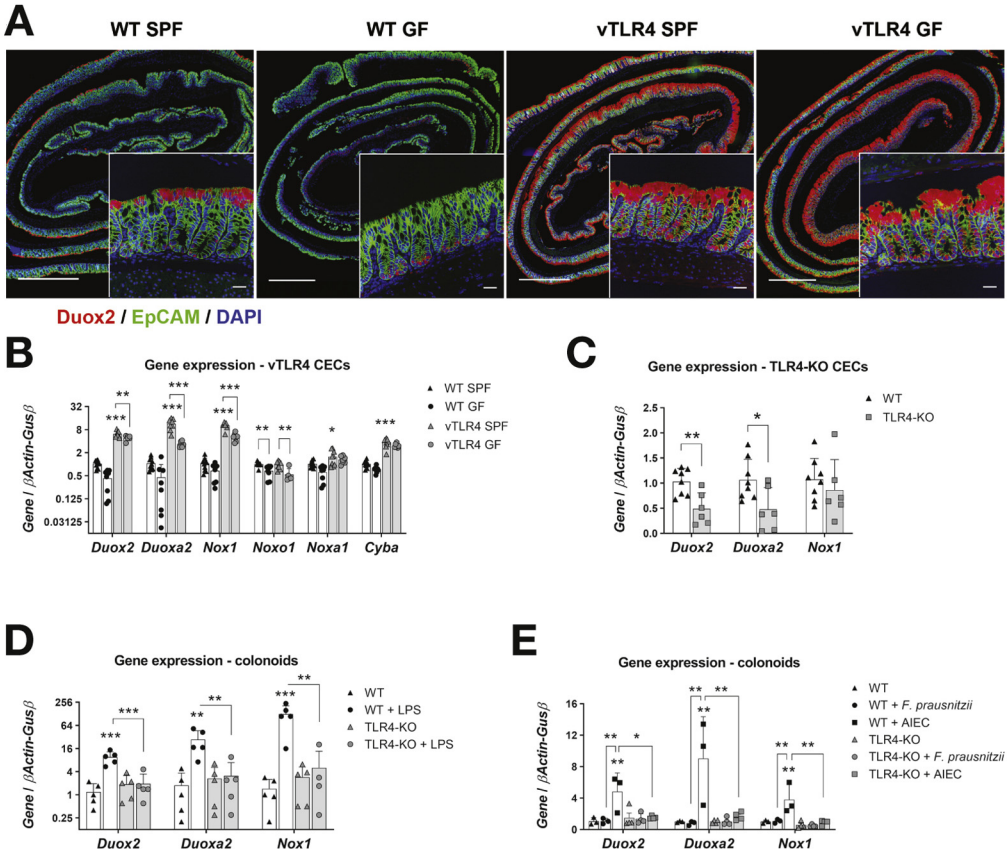


**Figure 2.** TLR4 controls the expression of epithelial *Duox2* and *Nox1*. (*A*) Representative *micrographs* show *Duox2* transcripts (*red*) counterstained with epithelial cell adhesion molecule (*green*) and 4′,6-diamidino-2-phenylindole (*blue*). *Micrograph* scale bar = 1 mm; *inset* scale bar = 25 $\mu$m. (*B*) Freshly isolated CECs were analyzed by quantitative PCR for the expression of selected transcripts. Villin-TLR4 SPF CECs showed increased expression of *Duox2*, *Duoxa2*, *Nox1*, *Cyba* (***$P < .001$), and *Noxa1* (*$P < .05$) compared with wild-type (WT) SPF CECs (n = 8–10 mice). Data were analyzed by 2-way analysis of variance (ANOVA) followed by Sidak's post-hoc test for each gene. "Microbiota" (SPF vs GF) was identified as a significant source of variation in the expression of *Duox2*, *Duoxa2*, *Nox1*, and *Noxo1* (all, $P < .001$), *Noxa1*, and *Cyba* (both, $P < .05$); n = 6–10 mice. (*C*) Gene expression in freshly isolated CECs of TLR4-KO and WT mice. *Duox2* (**$P < .01$) and *Duoxa2* (*$P < .05$) were significantly down-regulated in TLR4-KO CECs (n = 6–8 mice). Data were analyzed by unpaired *t* test for each gene. (*D*) Cultured WT and TLR4-KO colonoids were stimulated with LPS for 24 hours and their gene expression was determined by quantitative PCR. *Duox2*, *Nox1* (***$P < .001$), and *Duoxa2* (**$P < .01$) transcripts were significantly up-regulated by LPS in WT colonoids (n = 5 cultures). Data were analyzed by 2-way ANOVA followed by Sidak's post-hoc test for each gene. (*E*) Cultured WT and TLR4-KO colonoids were stimulated with heat-killed *F prausnitzii* or AIEC for 24 hours and their gene expression was determined by quantitative PCR. *Duox2*, *Duoxa2*, and *Nox1* (**$P < .01$) transcripts were significantly up-regulated by AIEC in WT colonoids (n = 3–4 cultures). Data were analyzed by 2-way ANOVA followed by Sidak's post-hoc test for each gene.

between "time" and "TLR4 activation" factors ($P < .05$), demonstrating that the release of $H_2O_2$ increased at higher rates in villin-TLR4 mice during the CAC model. The positive correlation between $H_2O_2$ production and histologic score ($r = 0.837$, $P < .0001$; Figure 4*F*) suggests that CEC-mediated $H_2O_2$ production is linked to the severity of dysplasia and tumorigenesis.

## *Both DUOX2 Signaling and the Microbiome Are Required for Toll-Like Receptor-4–Dependent Colonic Tumorigenesis*

The correlation between epithelial $H_2O_2$ production and histologic score led us to hypothesize that epithelial ROS participate in tumor initiation and progression. To test this hypothesis, we used repeated administration of AOM, without DSS, as a model of CRC to mitigate the confounding effect of ROS from mucosal phagocytic cells. This model is analogous to patients with dysplasia in the absence of active inflammation. We have previously shown that villin-TLR4 mice develop tumors with AOM alone by 17 weeks, whereas wild-type C57/Bl6 mice require more than 30 weeks.[25,38] To investigate the involvement of epithelial ROS and particularly DUOX2 in this model, we backcrossed villin-TLR4 mice to DUOXA-KO mice and compared adenoma formation (Figure 5*A*). Genetic deletion of DUOXA led to a significant reduction in *Duox2* expression (Figure 5*B*), which was found essentially at the tips of the crypts (Figure 5*D, upper panels*) and caused a decrease in the production of $H_2O_2$ by CECs (Figure 5*C*). Villin-TLR4 DUOXA-KO mice developed fewer tumors, of smaller size, compared with villin-TLR4 littermates (Figure 5*D*, *H&E panel*, and *E*). These

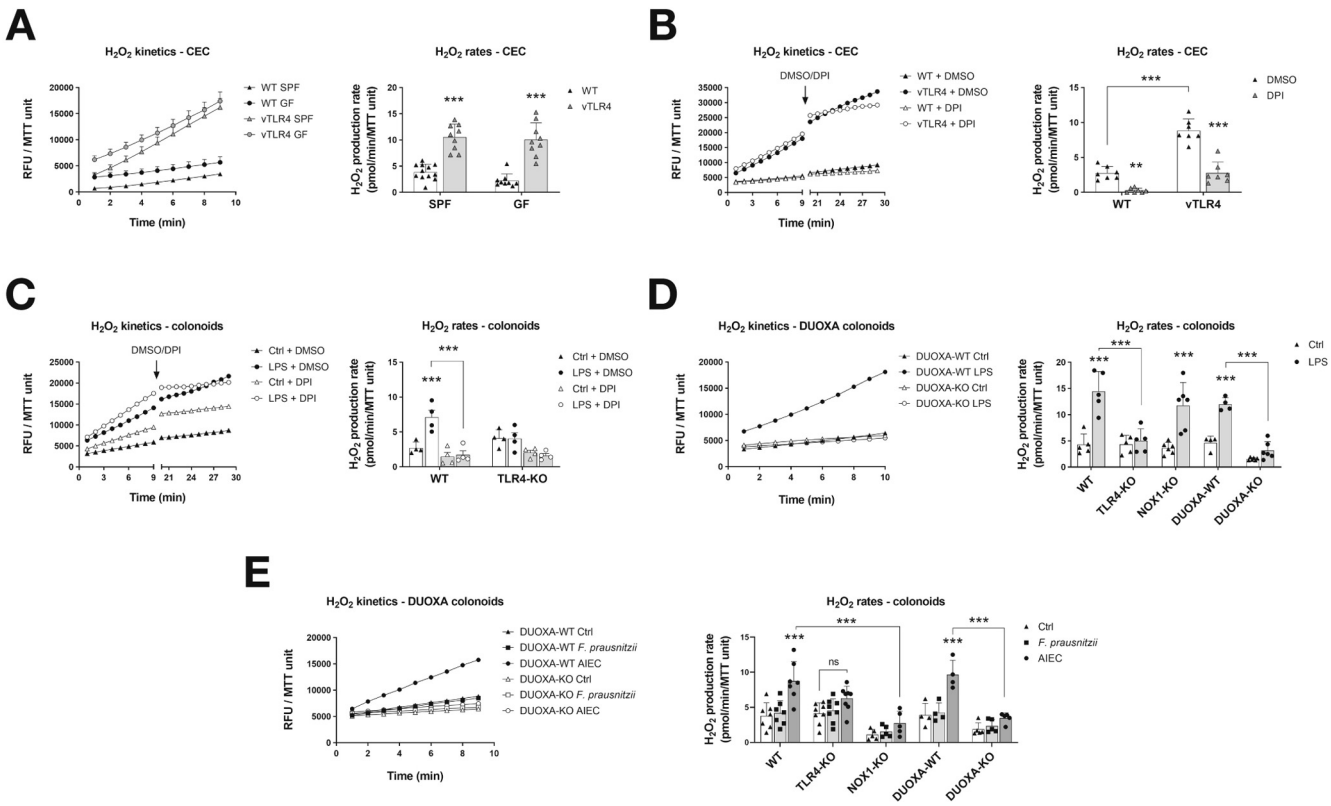


**Figure 3.** Activation of TLR4 induces epithelial production of $H_2O_2$ via DUOX2. *Left panels* show kinetic production of $H_2O_2$ in 1 representative experiment expressed in relative fluorescence units (RFU) normalized to MTT viability values. *Right panels* show the $H_2O_2$ production rate in all experiments. (*A*) Freshly isolated CECs were assayed for the kinetic production of $H_2O_2$ in SPF and GF-raised villin-TLR4 mice and littermates. Villin-TLR4 mice had increased $H_2O_2$ production rates (***$P < .001$) compared with wild-type (WT) littermates (n = 9–12 mice). (*B*) We tested the effects of NADPH oxidase inhibition in freshly isolated CECs by adding DPI or dimethyl sulfoxide after 9 minutes of kinetic determination and measuring for 10 additional minutes. DPI markedly reduced $H_2O_2$ production in WT (**$P < .01$) and villin-TLR4 (***$P < .001$) CECs (n = 7 mice). (*C*) Production of $H_2O_2$ was determined in WT and TLR4-KO colonoids stimulated for 24 hours with LPS. *Left panel* shows $H_2O_2$ production kinetics in WT organoids. LPS stimulation induced a release of $H_2O_2$ in WT colonoids (***$P < .001$) that was completely abrogated by DPI (***$P < .001$; n = 4 cultures). (*D*, *E*) TLR4-KO, DUOXA-KO, and NOX1-KO colonoids were stimulated with LPS (n = 4–6 cultures), *F prausnitzii*, or AIEC (n = 4–9 cultures) and their release of $H_2O_2$ was determined (***$P < .001$). Data in all figures were analyzed by 2-way analysis of variance followed by Sidak's post-hoc test.

findings demonstrate that activation of DUOX2 and production of epithelial ROS in response to microbial stimuli are required for the development of colonic neoplasia.

We next sought to determine whether epithelial TLR4-induced ROS are sufficient to induce tumorigenesis or whether there is a requirement for the microbiota. To answer this question, we compared the development of tumors in villin-TLR4 mice raised in GF vs SPF conditions (Figure 5*F*). Consistent with our published findings,[25] neither wild-type SPF nor wild-type GF mice undergoing this model developed colon adenomas (Figure 5*G*). Villin-TLR4 mice raised in SPF conditions developed tumors in 100% of cases (5 of 5 mice). However, villin-TLR4 mice under GF conditions were significantly protected from AOM-induced tumors; only 1 tumor developed in 1 mouse of 8 (12.5%) ($P < .01$; Figure 5*G*), demonstrating that TLR4-mediated susceptibility to tumorigenesis is dependent on the microbiota. To address the involvement of epithelial ROS in tumor initiation in this CRC model, we analyzed the $H_2O_2$ production in CECs isolated from nontumor areas. Although $H_2O_2$ production in CECs from villin-TLR4 kept in GF conditions was higher than in villin-TLR4 SPF mice (Figure 5*H*), villin-TLR4 GF mice did not develop adenomas (Figure 5*G*). These findings demonstrate that TLR4 signaling drives epithelial ROS even under GF conditions, but is not sufficient to initiate tumorigenesis in the absence of the microbiota.

## *Toll-Like Receptor 4–Shaped Microbiota Transfers Epithelial Redox Activity and Susceptibility to Tumorigenesis*

We show above that both epithelial ROS and the microbiota interact to accelerate tumorigenesis in villin-TLR4 mice. We have previously shown that TLR4 expression in the epithelium shapes the mucosa-associated microbiota and can transfer susceptibility to colitis.[27] We next asked whether the microbiota of villin-TLR4 mice could transfer the susceptibility to tumors. To determine whether TLR4-shaped microbiota promotes tumorigenesis, wild-type GF mice were orally gavaged with the mucosa-associated

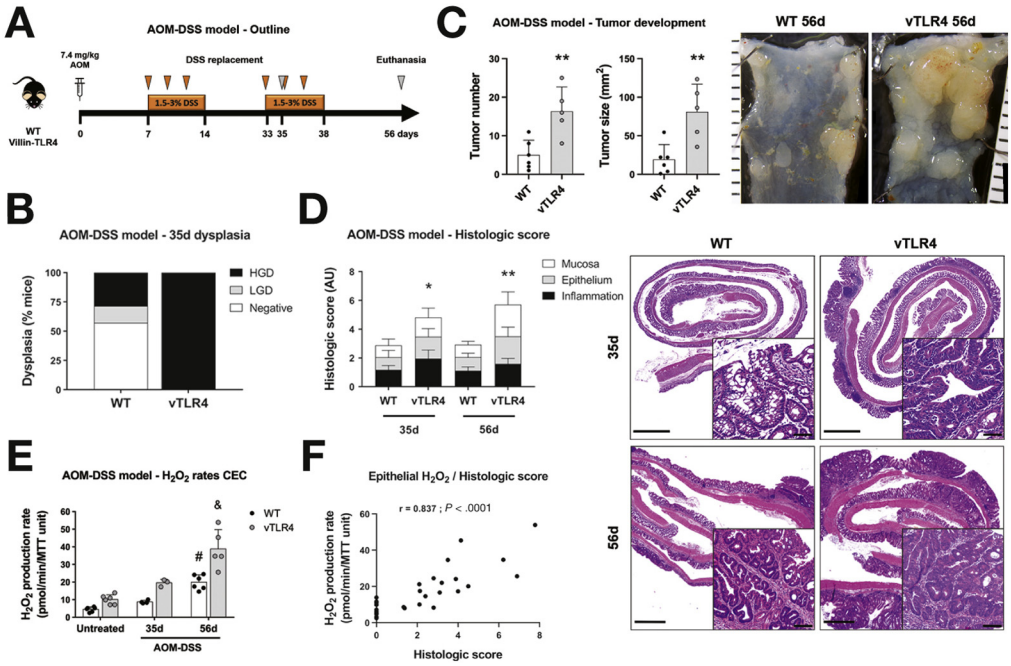


**Figure 4.** Epithelial release of $H_2O_2$ is sequentially increased in the different phases of tumor development. (*A*) Villin-TLR4 mice and their wild-type (WT) littermates underwent the AOM-DSS model of CAC for 35 or 56 days. (*B*) Percentage of mice that developed no dysplasia (negative), low-grade dysplasia (LGD), or high-grade dysplasia (HGD) at 35 days (n = 7 mice). Dysplasia (LGD+HGD) was compared between groups by chi-square test. (*C*) Tumor number and size (**$P < .01$) were increased in villin-TLR4 compared with WT mice after a 56d-CAC model (n = 5–6 mice). *Micrographs* show representative distal colons of each group of mice; scale bar in mm. (*D*) Histologic score was increased in villin-TLR4 mice compared with WT littermates on days 35 (*$P < .05$; n = 7 mice) and 56 (**$P < .01$; n = 5–6 mice). *Right panels* show representative micrographs for WT and villin-TLR4 mice colon at both times. *Micrograph* scale bar = 1 mm; *inset* scale bar = 50 $\mu$m. (*E*) Epithelial $H_2O_2$ production rate in freshly isolated CECs throughout the CAC model. (#) WT-56d vs WT-untreated (***$P < .001$) and WT-56d vs WT-35d (*$P < .05$); (&) vTLR4-56d vs vTLR4-untreated (***$P < .001$), vTLR4-56d vs vTLR4-35d (***$P < .001$); and vTLR4-56d vs WT-56d (***$P < .001$; n = 3–6 mice). "Time" ($P < .001$), "TLR4 activation" ($P < .001$), and the interaction between these ($P < .05$) were also identified as significant variation factors in epithelial release of $H_2O_2$. (*F*) Spearman correlation between histologic score and CEC $H_2O_2$ production ($r = 0.837$; $P < .0001$; n = 30 mice).



microbiota of wild-type vs villin-TLR4 mice and underwent the AOM-DSS model of CAC (Figure 6*A*). Three weeks after the initial engraftment, a small group of mice were euthanized to analyze the engraftment stability using 16s ribosomal RNA sequencing of donor and recipient mucosa-associated microbiota samples. Wild-type donor microbiota had a ≥88% engraftment at the phylum, class, and genus levels, while villin-TLR4 microbiota had a ≥70% engraftment (Supplementary Table 2). We did not find significant differences between wild-type and villin-TLR4 mice with respect to the overall community structure of the microbiota (Supplementary Figure 5).

Wild-type GF mice receiving the mucosa-associated microbiota of villin-TLR4 donors developed more and larger tumors than wild-type recipients of wild-type microbiota (Figure 6*B*), as well as more severe histologic lesions (Figure 6*C*), emulating the villin-TLR4 phenotype. Moreover, transfer of villin-TLR4–derived microbiota was also associated with a higher rate of $H_2O_2$ synthesis by CECs (Figure 6*D*), suggesting that TLR4-shaped microbiota enhances susceptibility to tumorigenesis and induces redox activity in the mucosa that might provide a feed forward loop for tumorigenesis. These results demonstrate that TLR4 signaling affects the functional properties of the microbiota, imbuing the ability to enhance $H_2O_2$ production and tumorigenesis.

## Discussion

The incidence of colon cancer in IBD continues to be higher than the general population, and death from colon cancer is also 2-fold higher in spite of earlier-stage cancer at diagnosis.[2] These observations compel us to identify targetable pathways that can alter the natural history of the disease. Here, we show that TLR4 up-regulation is a common feature in tissues from IBD and CRC patients and is accompanied by increases in expression of *DUOX2*. We mimicked this observation in diverse experimental models to understand the mechanistic implications. We demonstrate that activation of TLR4 and DUOX2 increases the production of $H_2O_2$ by CECs, which in turn promotes tumor initiation (a greater number) and progression (larger, higher grades of dysplasia). Using mucosa-associated microbiota from tumor-prone villin-TLR4 mice, we further show that the microbiota functionally transmit susceptibility to tumorigenesis and production of epithelial ROS. In clinical terms, the implication is that host innate immune responses and the mucosa-associated microbiota are necessary

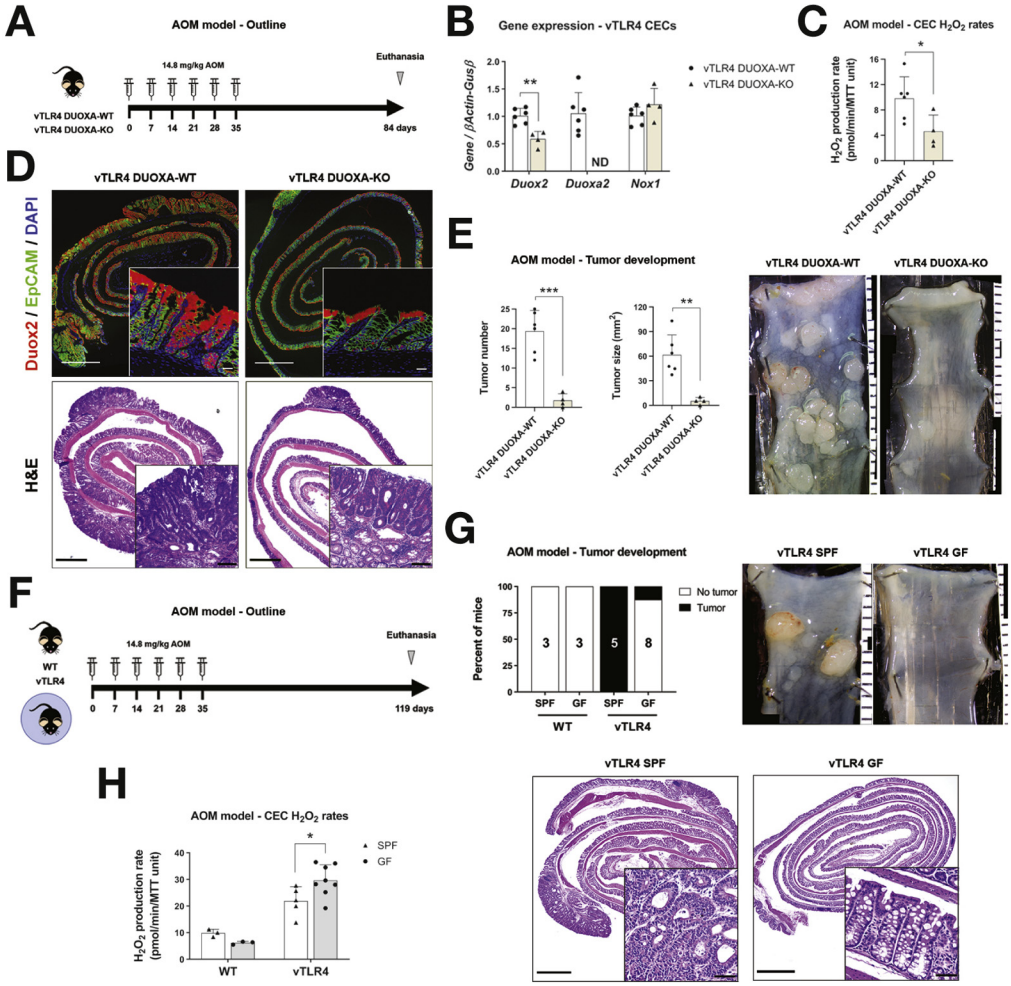


**Figure 5.** Epithelial DUOX2 and TLR4-shaped microbiota induce tumor initiation. (*A*) Villin-TLR4 DUOXA-KO and their villin-TLR4 littermates underwent the AOM model of CRC for 12 weeks. (*B*) Gene expression in CECs. Deletion of *Duoxa* (nondetectable [ND]) caused a significant down-regulation of *Duox2* (**$P < .01$; n = 4–6 mice). (*C*) CEC production of $H_2O_2$ in villin-TLR4 mice was reduced by deletion of DUOXA (*$P < .05$; n = 4–6 mice). (*D*) Representative *micrographs* of *Duox2* in situ hybridization and H&E for AOM-treated villin-TLR4 mice. *Micrograph* scale bar = 1 mm; *inset* scale bar = 25 $\mu$m and 50 $\mu$m, respectively. (*E*) Tumor number (***$P < .001$) and size (**$P < .01$) were decreased in villin-TLR4 lacking DUOXA (n = 4–6 mice). *Micrographs* show representative distal colons of each group of mice; scale bar in mm. (*F*) Villin-TLR4 mice and their wild-type (WT) littermates raised in SPF and GF conditions underwent the AOM model of CRC for 17 weeks. (*G*) Percentage of mice developing tumors in each condition is shown in *black* (n = 3–8 mice). Tumor development was compared between groups by chi-square test. Representative *micrographs* of AOM-treated villin-TLR4 mice grown in SPF and GF conditions. *Micrograph* scale bar = 1 mm; inset scale bar = 50 $\mu$m. (*H*) Epithelial $H_2O_2$ production rate at the time of euthanasia (n = 3–8 mice). Villin-TLR4-SPF vs villin-TLR4-GF, * $P < .05$, as determined by 2-way analysis of variance followed by Sidak's post-hoc test.

co-conspirators in the development of dysplasia and ultimately cancer.

Our laboratory has carefully characterized the involvement of TLR4 in colon cancer. In human tissue microarrays, we described that TLR4 expression increases specifically in CECs as tissues progress from normal to neoplastic stages.[25,26] Subsequently, we demonstrated that epithelial TLR4 deficiency protected mice from CAC[39] and that overactivation of this receptor led to increased susceptibility to CAC and CRC.[25,28] Here, we show that epithelial TLR4 signaling triggers an oxidative program characterized by a marked increase in DUOX2 expression in human samples and mice. Functionally, the up-regulation of DUOX2 translates into enhanced epithelial redox activity that, in the presence of a microbiota, promotes the development of tumors. Given the proximity between DUOX2 (top of the crypts) and the mucosa-associated microbiota and our findings in villin-TLR4 GF mice treated with AOM, we believe that DUOX2 shapes the microbiota to confer pro-tumorigenic properties. Previous studies have proposed that epithelial ROS can alter the gut microbiota either at a compositional[40] or functional level.[14,15] We did not find significant differences in the community structure of the mucosa-associated microbiota between wild-type and villin-TLR4 mice, suggesting that functional alterations in the microbiota are responsible for the increased pro-tumorigenic activity. Traditionally, ROS has been implicated in activating redox signaling pathways in stem cells[41] and it is possible that epithelial TLR4-dependent ROS contributes to

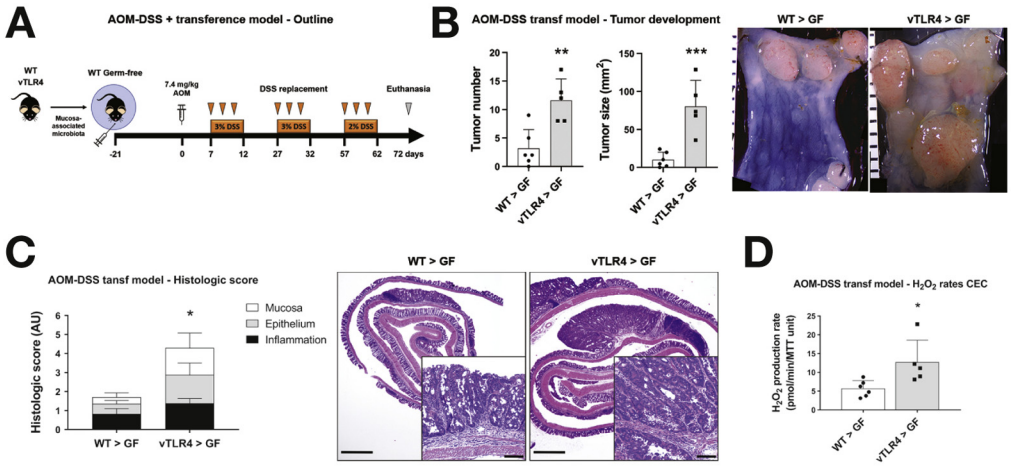


**Figure 6.** TLR4-shaped microbiota transfers tumor susceptibility to wild-type (WT) mice. (*A*) The mucosa-associated microbiota of villin-TLR4 and WT mice were used to colonize WT GF mice that subsequently underwent the AOM-DSS CAC model. (*B*) Tumor number (**$P < .01$) and size (***$P < .001$) in GF mice receiving WT (WT > GF) or villin-TLR4 (vTLR4 > GF) microbiota (n = 5–6 recipient GF mice). *Micrographs* show representative distal colons of each group of mice; scale bar in mm. (*C*) Histologic score was increased in vTLR4 > GF mice compared with WT > GF littermates (*$P < .05$; n = 5–6 mice). Representative *micrographs* show tumor development in mice. *Micrograph* scale bar = 1 mm; *inset* scale bar = 50 $\mu$m. (*D*) Epithelial $H_2O_2$ production rate at the time of euthanasia (*$P < .05$; n = 5–6 mice).

this mechanism as well. Deeper studies will be necessary to identify potential modifications and culprits in the host and the microbiota with tumor promoting properties. Ultimately, these findings have important implications in the design of new therapeutic approaches to prevent dysplastic progression and suggest that therapeutic strategies need to address the host's antimicrobial response to mitigate the risk of CRC.[42,43]

Our study corroborates that DUOX2 is up-regulated in IBD[11,20] and extends it to CRC. We showed a direct link between recognition of Gram-negative bacteria via TLR4 and regulation of DUOX2 activity and subsequent production of epithelial $H_2O_2$. Although we also observed an up-regulation of NOX1, we focused on DUOX2 because we and others have previously shown that TLR4 and IBD dysbiosis up-regulate *Duox2*[21] and increase the production of epithelial $H_2O_2$ in GF mice.[22] Now, we showed that dysregulation of this NADPH oxidase is necessary but not sufficient to cause tumors, and that the presence of the microbiota is also required to cause dysplasia. Taken together, our previous and current data support an interactive feedback loop: TLR4 activation leading to increased ROS, ROS-mediated modification of the microbiome that, in turn, further enhances DUOX2 activity and $H_2O_2$ production. Interestingly, in vitro, IBD-protective bacteria such as *F prausnitzii* do not induce $H_2O_2$ production and might constitute an approach to ameliorating the functional tumorigenic properties of the microbiome. Our experiments also indicate that overt inflammation is not necessary to generate local $H_2O_2$ or cause tumors. Indeed, villin-TLR4 mice do not display signs of inflammation in steady-state conditions.[25] These findings suggest that increased epithelial TLR4 signaling, even during remission, could participate in perpetuating local $H_2O_2$, dysbiosis,[13,40] and, therefore, increase the chances of developing dysplasia.

In summary, we showed the mechanistic link between TLR4 activation and microbiota and tumorigenesis. Although our mouse model and in vitro system focused on TLR4, we believe this is a model for increased TLR signaling more broadly. Our results suggest that we must develop strategies to target common pathways in TLR signaling and, at the same time, address the tumor-promoting microbiota. Because the process is driven by epithelial TLR signaling, it is theoretically possible that localized inhibitors of TLR signaling can be developed without incurring the potential risk of systemic TLR inhibition. Our studies also help to shed light on why certain patients develop dysplasia long after the active inflammation has been treated. We believe that selective targeting of ROS pathways and microbiome-based approaches need to be delivered simultaneously to mitigate dysplasia in IBD patients, even in those in endoscopic and histologic remission.

## Supplementary Material

Note: To access the supplementary material accompanying this article, visit the online version of *Gastroenterology* at www.gastrojournal.org, and at http://doi.org/10.1053/j.gastro.2020.10.031.

## References

1. Molodecky NA, Soon IS, Rabi DM, et al. Increasing incidence and prevalence of the inflammatory bowel diseases with time, based on systematic review. Gastroenterology 2012;142:46–54 e42; quiz e30.
2. **Olen O, Erichsen R**, Sachs MC, et al. Colorectal cancer in ulcerative colitis: a Scandinavian population-based cohort study. Lancet 2020;395(10218):123–131.

3. Ekbom A, Helmick C, Zack M, et al. Ulcerative colitis and colorectal cancer. A population-based study. N Engl J Med 1990;323:1228–1233.
4. Rubio CA, Befrits R. Colorectal adenocarcinoma in Crohn's disease: a retrospective histologic study. Dis Colon Rectum 1997;40:1072–1078.
5. Nowacki TM, Bruckner M, Eveslage M, et al. The risk of colorectal cancer in patients with ulcerative colitis. Dig Dis Sci 2015;60:492–501.
6. Watanabe T, Konishi T, Kishimoto J, et al. Ulcerative colitis-associated colorectal cancer shows a poorer survival than sporadic colorectal cancer: a nationwide Japanese study. Inflamm Bowel Dis 2011;17:802–808.
7. Munkholm P. Review article: the incidence and prevalence of colorectal cancer in inflammatory bowel disease. Aliment Pharmacol Ther 2003;18(Suppl 2):1–5.
8. Chu H, Khosravi A, Kusumawardhani IP, et al. Gene-microbiota interactions contribute to the pathogenesis of inflammatory bowel disease. Science 2016;352:1116–1120.
9. Schirmer M, Garner A, Vlamakis H, et al. Microbial genes and pathways in inflammatory bowel disease. Nat Rev Microbiol 2019;17:497–511.
10. Richard ML, Liguori G, Lamas B, et al. Mucosa-associated microbiota dysbiosis in colitis associated cancer. Gut Microbes 2018;9:131–142.
11. Lloyd-Price J, Arze C, Ananthakrishnan AN, et al. Multi-omics of the gut microbial ecosystem in inflammatory bowel diseases. Nature 2019;569:655–662.
12. Fritsch J, Abreu MT. The microbiota and the immune response: what is the chicken and what is the egg? Gastrointest Endosc Clin N Am 2019;29:381–393.
13. Zhu W, Winter MG, Byndloss MX, et al. Precision editing of the gut microbiota ameliorates colitis. Nature 2018;553:208–211.
14. Alvarez LA, Kovacic L, Rodriguez J, et al. NADPH oxidase-derived H2O2 subverts pathogen signaling by oxidative phosphotyrosine conversion to PB-DOPA. Proc Natl Acad Sci U S A 2016;113:10406–10411.
15. **Corcionivoschi N, Alvarez LA**, Sharp TH, et al. Mucosal reactive oxygen species decrease virulence by disrupting *Campylobacter jejuni* phosphotyrosine signaling. Cell Host Microbe 2012;12:47–59.
16. Grasberger H, El-Zaatari M, Dang DT, et al. Dual oxidases control release of hydrogen peroxide by the gastric epithelium to prevent *Helicobacter felis* infection and inflammation in mice. Gastroenterology 2013;145:1045–1054.
17. Levine AP, Pontikos N, Schiff ER, et al. Genetic complexity of Crohn's disease in two large Ashkenazi Jewish families. Gastroenterology 2016;151:698–709.
18. **Hayes P, Dhillon S**, O'Neill K, et al. Defects in NADPH oxidase genes NOX1 and DUOX2 in very early onset inflammatory bowel disease. Cell Mol Gastroenterol Hepatol 2015;1:489–502.
19. Parlato M, Charbit-Henrion F, Hayes P, et al. First identification of biallelic inherited DUOX2 inactivating mutations as a cause of very early onset inflammatory bowel disease. Gastroenterology 2017;153:609–611.e3.
20. Haberman Y, Tickle TL, Dexheimer PJ, et al. Pediatric Crohn disease patients exhibit specific ileal transcriptome and microbiome signature. J Clin Invest 2014;124:3617–3633.
21. Grasberger H, Gao J, Nagao-Kitamoto H, et al. Increased expression of DUOX2 is an epithelial response to mucosal dysbiosis required for immune homeostasis in mouse intestine. Gastroenterology 2015;149:1849–1859.
22. **Burgueno JF, Fritsch J**, Santander AM, et al. Intestinal epithelial cells respond to chronic inflammation and dysbiosis by synthesizinf H2O2. Front Physiol 2019;10:1484.
23. Medzhitov R, Preston-Hurlburt P, Janeway CA Jr. A human homologue of the Drosophila Toll protein signals activation of adaptive immunity. Nature 1997;388:394–397.
24. Burgueno JF, Abreu MT. Epithelial Toll-like receptors and their role in gut homeostasis and disease. Nat Rev Gastroenterol Hepatol 2020;17:263–278.
25. Santaolalla R, Sussman DA, Ruiz JR, et al. TLR4 activates the beta-catenin pathway to cause intestinal neoplasia. PLoS One 2013;8:e63298.
26. Sussman DA, Santaolalla R, Bejarano PA, et al. In silico and ex vivo approaches identify a role for Toll-like receptor 4 in colorectal cancer. J Exp Clin Cancer Res 2014;33:45.
27. Dheer R, Santaolalla R, Davies JM, et al. Intestinal epithelial Toll-like receptor 4 signaling affects epithelial function and colonic microbiota and promotes a risk for transmissible colitis. Infect Immun 2016;84:798–810.
28. Fukata M, Shang L, Santaolalla R, et al. Constitutive activation of epithelial TLR4 augments inflammatory responses to mucosal injury and drives colitis-associated tumorigenesis. Inflamm Bowel Dis 2011;17:1464–1473.
29. Shang L, Fukata M, Thirunarayanan N, et al. Toll-like receptor signaling in small intestinal epithelium promotes B-cell recruitment and IgA production in lamina propria. Gastroenterology 2008;135:529–538.
30. **Burgueno JF, Lang JK**, Santander AM, et al. Fluid supplementation accelerates epithelial repair during chemical colitis. PLoS One 2019;14:e0215387.
31. Fukata M, Chen A, Vamadevan AS, et al. Toll-like receptor-4 promotes the development of colitis-associated colorectal tumors. Gastroenterology 2007;133:1869–1881.
32. Kugathasan S, Baldassano RN, Bradfield JP, et al. Loci on 20q13 and 21q22 are associated with pediatric-onset inflammatory bowel disease. Nat Genet 2008;40:1211–1215.
33. Sabates-Bellver J, Van der Flier LG, de Palo M, et al. Transcriptome profile of human colorectal adenomas. Mol Cancer Res 2007;5:1263–1275.
34. Grasberger H, Refetoff S. Identification of the maturation factor for dual oxidase. Evolution of an eukaryotic operon equivalent. J Biol Chem 2006;281:18269–18272.
35. Panday A, Sahoo MK, Osorio D, et al. NADPH oxidases: an overview from structure to innate immunity-associated pathologies. Cell Mol Immunol 2015;12:5–23.
36. Sokol H, Pigneur B, Watterlot L, et al. *Faecalibacterium prausnitzii* is an anti-inflammatory commensal bacterium identified by gut microbiota analysis of Crohn disease

patients. Proc Natl Acad Sci U S A 2008;105:16731–16736.
37. Palmela C, Chevarin C, Xu Z, et al. Adherent-invasive *Escherichia coli* in inflammatory bowel disease. Gut 2018;67:574–587.
38. Neufert C, Becker C, Neurath MF. An inducible mouse model of colon carcinogenesis for the analysis of sporadic and inflammation-driven tumor progression. Nat Protoc 2007;2:1998–2004.
39. Fukata M, Hernandez Y, Conduah D, et al. Innate immune signaling by Toll-like receptor-4 (TLR4) shapes the inflammatory microenvironment in colitis-associated tumors. Inflamm Bowel Dis 2009;15:997–1006.
40. Winter SE, Lopez CA, Baumler AJ. The dynamics of gut-associated microbial communities during inflammation. EMBO Rep 2013;14:319–327.
41. Holmstrom KM, Finkel T. Cellular mechanisms and physiological consequences of redox-dependent signalling. Nat Rev Mol Cell Biol 2014;15:411–421.
42. **Coleman OI, Lobner EM**, Bierwirth S, et al. Activated ATF6 induces intestinal dysbiosis and innate immune response to promote colorectal tumorigenesis. Gastroenterology 2018;155:1539–1552 e12.
43. Zhu W, Miyata N, Winter MG, et al. Editing of the gut microbiota reduces carcinogenesis in mouse models of colitis-associated colorectal cancer. J Exp Med 2019;216:2378–2393.



**Author names in bold designate shared co-first authorship.**

**Received December 12, 2019. Accepted October 20, 2020.**

**Correspondence**
Address correspondence to: Maria T. Abreu, MD, Department of Medicine, Division of Gastroenterology, University of Miami–Miller School of Medicine, 1011 NW 15th Street (D-149), Gautier Building, Suite 510, Miami, Florida 33136. e-mail: Mabreu1@med.miami.edu.

**Acknowledgments**
The authors acknowledge Dr Kaunitz and Dr Akiba at UCLA for generating and providing the original DUOXA epithelial knockout mice. The authors also acknowledge Dr Sokol, Dr Rolhion, and Ms Straube at Sorbonne Université (INSERM) for providing heat-killed *Faecalibacterium prausnitzii* and adherent invasive *Escherichia coli*. Graphical abstract was created with BioRender.com.

Transcript profiling: GSE141767 microarray data are available at https://www.ncbi.nlm.nih.gov/geo/query/acc.cgi?acc=GSE141767.

**CRediT Authorship Contributions**
Juan F. Burgueno, DVM, PhD (Conceptualization: Lead; Data curation: Equal; Formal analysis: Lead; Investigation: Lead; Methodology: Equal; Visualization: Equal; Writing – original draft: Lead; Writing – review & editing: Equal)

Julia Fritsch, PhD (Conceptualization: Supporting; Data curation: Equal; Formal analysis: Supporting; Investigation: Supporting; Methodology: Supporting; Writing – original draft: Supporting; Writing – review & editing: Supporting)

Eddy E. Gonzalez, MS (Investigation: Supporting; Methodology: Supporting),

Kevin S. Landau, MD (Data curation: Equal; Software: Lead; Visualization: Supporting) Ana M. Santander, BS (Investigation: Supporting; Resources: Supporting),

Irina Fernandez, MS (Methodology: Lead; Resources: Equal),

Hajar Hazime, MS (Investigation: Supporting),

Julie M. Davies, PhD (Data curation: Equal; Investigation: Supporting; Methodology: Supporting),

Rebeca Santaolalla, PhD (Investigation: Supporting; Methodology: Supporting; Project administration: Supporting; Resources: Supporting; Supervision: Supporting)

Matthew C Phillips, MD, PhD (Investigation: Supporting)

Sophia Diaz, MD (Formal analysis: Supporting; Investigation: Supporting)

Rishu Dheer, PhD (Data curation: Supporting; Investigation: Supporting)

Nivis Brito, BS (Methodology: Supporting; Resources: Supporting),

Judith Pignac-Kobinger, MS (Project administration: Lead; Resources: Supporting; Supervision: Supporting)

Ester Fernandez, PhD (Investigation: Supporting; Supervision: Supporting; Validation:

Supporting; Writing – review & editing: Supporting)

Gregory E. Conner, PhD (Conceptualization: Supporting; Investigation: Supporting; Methodology: Equal; Supervision: Equal; Writing – review & editing: Supporting)

Maria T. Abreu, MD (Conceptualization: Lead; Funding acquisition: Lead; Supervision: Lead; Writing – review & editing: Lead).

**Conflicts of interest**
This author disclose the following: Maria T. Abreu has served as a consultant to Boehringer Ingelheim Pharmaceuticals, Gilead, Janssen, Abbvie, Eli Lilly and Landos Biopharma; as a trainer or lecturer for Imedex, Focus Medical Communications and Cornerstones Health, Inc; and has funded investigator-initiated projects by Pfizer, Prometheus Laboratories, and Takeda Pharmaceuticals. The remaining authors disclose no conflicts.

**Funding**
This work was supported by grants from the National Institute of Diabetes and Digestive and Kidney Diseases (R01DK099076), the Micky & Madeleine Arison Family Foundation Crohn's & Colitis Discovery Laboratory, and Martin Kalser Chair to Maria T. Abreu.

# Supplementary Methods

## Histologic Evaluation

Histologic assessment for the development of inflammation and dysplasia was performed by a pathologist blinded to the study design. A histopathologic score was built following criteria described previously.[e1] Briefly, a minimum of ten 20× power fields were evaluated for inflammatory cell infiltrate (inflammation), including density of infiltrates and layer extent; epithelial changes (epithelium), including hyperplasia and goblet cell loss; and mucosal architecture (mucosa), including ulceration, crypt loss, and irregular crypts. Dysplasia was classified as negative, low-grade dysplasia, or high-grade dysplasia, depending on nuclear atypism (polarization, stratification, and chromatism), epithelial differentiation, and abnormal growth patterns defined previously. [e2,e3]

## In Situ Hybridization and Immunofluorescence

In situ hybridization for *Duox2* and *Nox1* transcripts was performed in paraffin-embedded tissues by means of the RNAscope technology (Advanced Cell Diagnostics) per manufacturer's instructions and with minor modifications. Specific probes for mouse *Duox2* (403501) and *Nox1* (464651) were hybridized by means of the RNAscope 2.5 HD Detection Reagent-RED kit (Advanced Cell Diagnostics) and developed using the Vector Red substrate kit (Vector Laboratories). Subsequently, samples were incubated overnight at 4°C with a primary rabbit polyclonal antibody against epithelial cell adhesion molecule (Abcam), followed by a secondary Alexa Fluor 488 goat anti-rabbit IgG polyclonal antibody (ThermoFisher Scientific) for 2 hours at room temperature. After staining nuclei with 4′,6-diamidino-2-phenylindole (ThermoFisher Scientific), slides were mounted with the Vectashield Hardset mounting medium (Vector Laboratories) and imaged under a BZ-X700 microscope (Keyence).

## Quantitative Polymerase Chain Reaction Analysis and Microarray

RNA from colon tissue, intestinal epithelial cells, and organoids was isolated by using the phenol-chloroform extraction method.[e4] Five hundred or 100 ng of RNA were reverse transcribed using PrimeScript RT reagent Kit (Takara Bio Inc), and the resulting complementary DNA was then amplified on a LightCycler 480 II instrument (Roche Applied Science) using SYBR Premix Ex Taq (Takara). The primers used are shown in Supplementary Table 1. To verify the amplification products, a melting curve analysis for each reaction was generated. Messenger RNA expression levels were then calculated using the ΔΔCt method[e5] and normalized to the geometric mean of the housekeeping genes $\beta$-actin and glucuronidase-$\beta$.

For microarray determinations, total RNA of tumor surrounding areas was sent to Ocean Ridge Biosciences (ORB, Palm Beach Gardens, FL) for analysis using the Mouse Exonic Evidence-Based Oligonucleotide (MEEBO) microarray (Lot 20868). Total RNA was used to prepare biotin-labeled complementary RNA and double-stranded complementary DNA as described elsewhere.[e6,e7] Double-stranded complementary DNA was subsequently used as a template for the preparation of biotinylated complementary RNA, which was fragmented and loaded on the MEEBO microarray slides. After overnight hybridization on a Model 400 Hybridization Incubator (Scigene), slides were stained with Streptavidin-Alexa 647 (ThermoFisher Scientific) and scanned using an Axon GenePix 4000B scanner (Molecular Devices).

## DNA Extraction and 16S Ribosomal RNA Sequencing

Total bacterial DNA was extracted, quantified, and sequenced at the University of Minnesota Genomic Center, as described previously.[e8] Briefly, DNA was extracted using PowerSoil/fecal DNA Isolation Kit (MoBio Laboratories) and the 16S-V4 region was amplified using Meta_V4_515F and Meta_V4_806R primers, and KAPAHiFidelity Hot Start Polymerase PCR. After a first amplification, the products were diluted 1:100, 5 $\mu$L of which were used for the second round of amplification. Various different combinations of forward and reverse indexing primers were used for the second PCR. For sequencing, pooled samples were denatured with NaOH, diluted to 8 pM in Illumina's HT1 buffer, spiked with 15% PhiX, and denatured at 96°C for 2 minutes. A MiSeq600 cycle v3 kit was used to sequence the DNA, and Nextera adapter sequences were used for post-run trimming.

## Bioinformatics

Affymetrix MAS5 algorithm was used to process and normalize the microarray data from the GEO datasets (GSE10616,[32] GSE8671[33]). Gene set enrichment analysis was performed using software from the Broad Institute of Massachusetts Institute of Technology and Harvard, [e9,e10] and the gene sets were acquired through the Molecular Signatures Database (MSigDB).[e11]

# Supplementary References


e1. Erben U, Loddenkemper C, Doerfel K, et al. A guide to histomorphological evaluation of intestinal inflammation in mouse models. Int J Clin Exp Pathol 2014;7:4557–4576.

e2. Riddell RH, Goldman H, Ransohoff DF, et al. Dysplasia in inflammatory bowel disease: standardized classification with provisional clinical applications. Hum Pathol 1983;14:931–968.

e3. Harpaz N, Polydorides AD. Colorectal dysplasia in chronic inflammatory bowel disease: pathology, clinical implications, and pathogenesis. Arch Pathol Lab Med 2010;134:876–895.

e4. Chomczynski P, Sacchi N. Single-step method of RNA isolation by acid guanidinium thiocyanate-phenol-chloroform extraction. Anal Biochem 1987;162:156–159.

e5. Livak KJ, Schmittgen TD. Analysis of relative gene expression data using real-time quantitative PCR and the 2(-Delta Delta C(T)) Method. Methods 2001;25:402–408.
e6. Van Gelder RN, Von Zastrow ME, Barchas JD, et al. Multi-Gene Expression ProfileVolume US7049102B1. Stanford, CA: Leland Stanford Junior University, 2006.
e7. Gubler U, Hoffman BJ. A simple and very efficient method for generating cDNA libraries. Gene 1983; 25:263–269.
e8. Gohl DM, Vangay P, Garbe J, et al. Systematic improvement of amplicon marker gene methods for increased accuracy in microbiome studies. Nat Biotechnol 2016;34:942–949.
e9. Mootha VK, Lindgren CM, Eriksson KF, et al. PGC-1alpha-responsive genes involved in oxidative phosphorylation are coordinately downregulated in human diabetes. Nat Genet 2003;34:267–273.
e10. Subramanian A, Tamayo P, Mootha VK, et al. Gene set enrichment analysis: a knowledge-based approach for interpreting genome-wide expression profiles. Proc Natl Acad Sci U S A 2005;102:15545–15550.
e11. Liberzon A, Subramanian A, Pinchback R, et al. Molecular signatures database (MSigDB) 3.0. Bioinformatics 2011;27:1739–1740.
e12. Bamias G, Okazawa A, Rivera-Nieves J, et al. Commensal bacteria exacerbate intestinal inflammation but are not essential for the development of murine ileitis. J Immunol 2007;178:1809–1818.
e13. Wang F, Wang J, Liu D, et al. Normalizing genes for real-time polymerase chain reaction in epithelial and nonepithelial cells of mouse small intestine. Anal Biochem 2010;399:211–217.
e14. Ibi M, Matsuno K, Shiba D, et al. Reactive oxygen species derived from NOX1/NADPH oxidase enhance inflammatory pain. J Neurosci 2008; 28:9486–9494.
e15. Moll F, Walter M, Rezende F, et al. NoxO1 controls proliferation of colon epithelial cells. Front Immunol 2018;9:973.

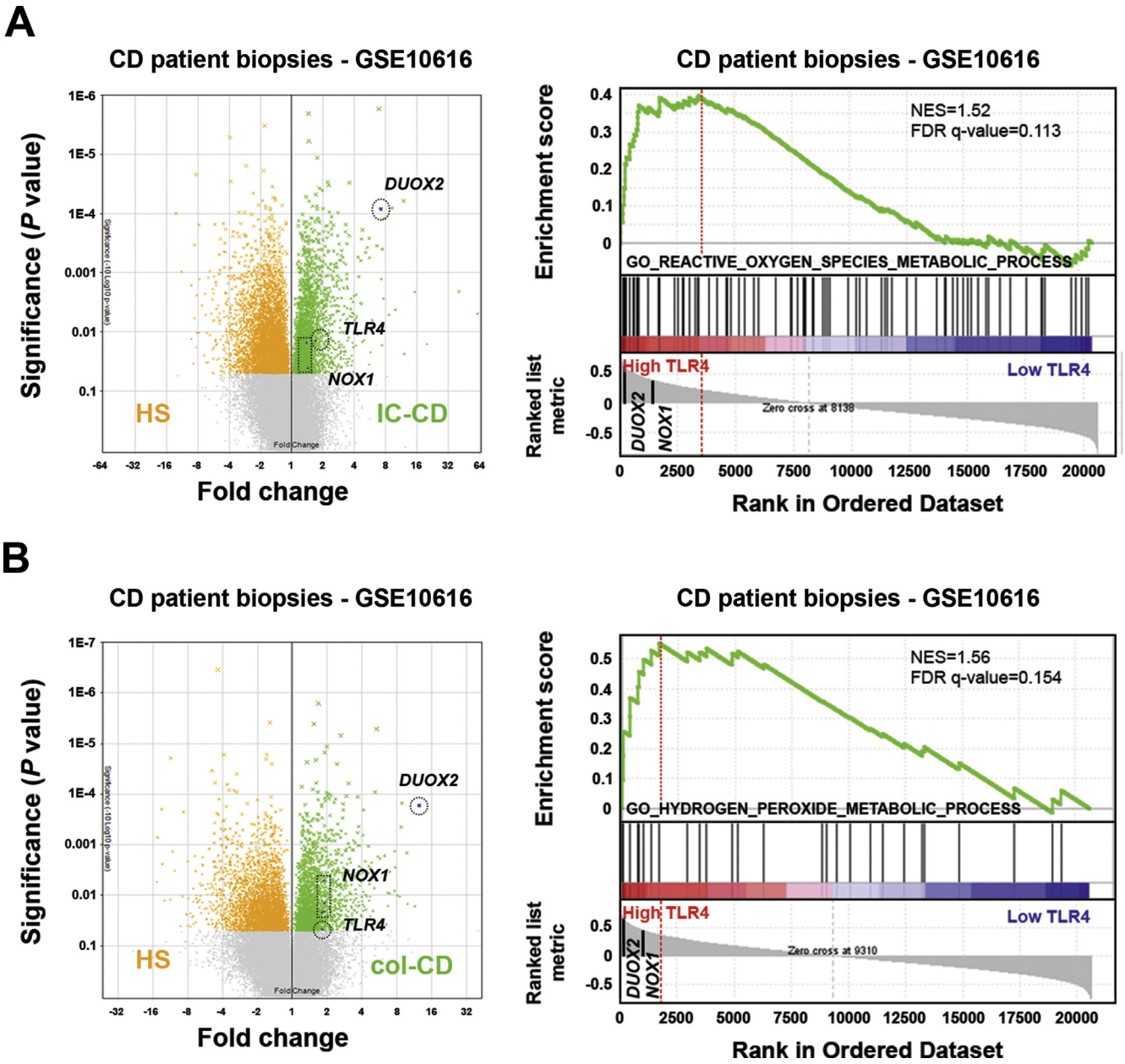


**Supplementary Figure 1.** Activation of TLR4 is associated with up-regulation of NADPH oxidases in Crohn's disease patients. (*A*) Expression of *TLR4*, *DUOX2*, and *NOX1* in the dataset GSE10616 of biopsies from patients with Crohn's disease. *Volcano plot* shows gene expression in patients with ileocolonic Crohn's disease (IC-CD) vs healthy subjects (HS). *Boxes* highlight the location of different probes for the same transcript. Gene set enrichment analysis (GSEA) plot shows that *DUOX2* and *NOX1* are in the leading-edge genes up-regulated in association with *TLR4* overexpression. (*B*) Expression of *TLR4*, *DUOX2*, and *NOX1* in the data set GSE10616 of biopsies from patients with Crohn's disease. *Volcano plot* shows gene expression in patients with colonic Crohn's disease (col-CD) vs healthy subjects (HS). *GSEA plot* shows that *DUOX2* and *NOX1* are in the leading-edge genes up-regulated in association with *TLR4* overexpression.

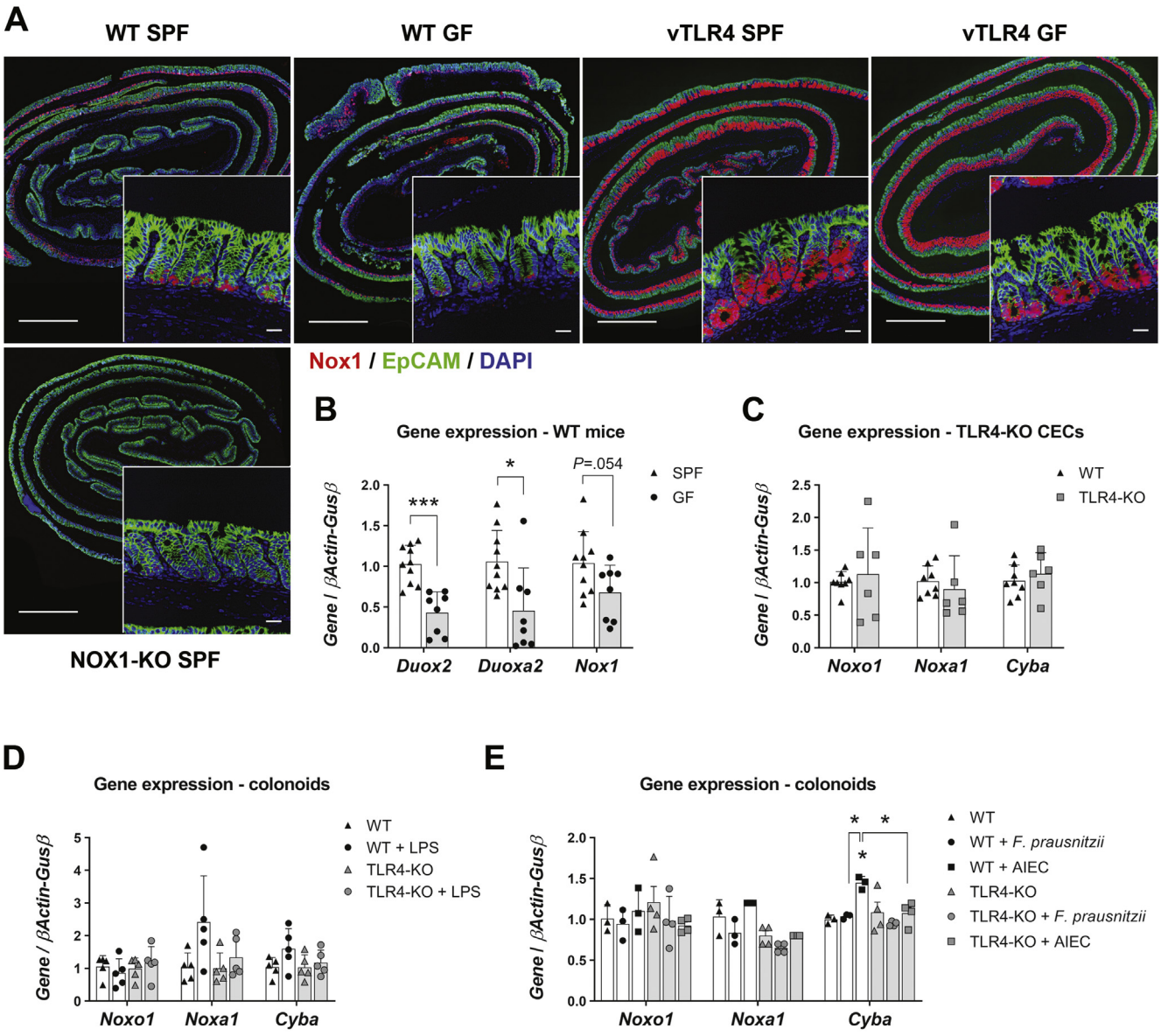


**Supplementary Figure 2.** The microbiota controls the expression of NADPH oxidases. (*A*) Representative *micrographs* show *Nox1* transcripts (*red*) counterstained with epithelial cell adhesion molecule (*green*) and 4′,6-diamidino-2-phenylindole (*blue*). *Micrograph* scale bar = 1 mm; *inset* scale bar = 25 $\mu$m. (*B*) Freshly isolated CECs were analyzed by quantitative PCR for the expression of selected transcripts. To interrogate the role of the microbiota in inducing NADPH oxidase gene expression, CECs from wild-type (WT) mice raised in SPF or GF conditions in Figure 2*B* were analyzed by means of an unpaired *t* test for each gene. *Duox2* (***$P < .001$), *Duoxa2* (*$P < .05$), and *Nox1* ($P = .054$) were down-regulated in the absence of a microbiota (n = 8–10 mice). (*C*) Expression of NOX1-associated genes was analyzed in freshly isolated WT and TLR4-KO CECs (n = 6–8 mice). (*D*) Expression of NOX1-associated genes was analyzed in wild-type and TLR4-KO colonoids stimulated with LPS for 24 hours (n = 5 cultures). (*E*) Expression of NOX1-associated genes was analyzed in WT and TLR4-KO colonoids stimulated with heat-killed *F prausnitzii* or AIEC for 24 hours (n = 5 cultures). AIEC induced expression of *Cyba* in WT, but not TLR4-KO colonoids (*$P < .05$).

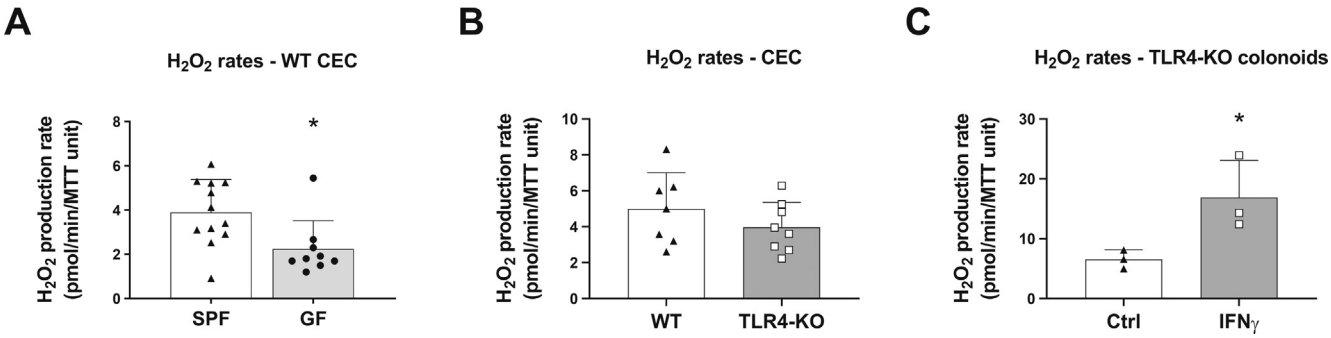


**Supplementary Figure 3.** TLR4 and the microbiota induce the production of epithelial $H_2O_2$. (*A*) To interrogate the role of the microbiota in inducing epithelial $H_2O_2$, freshly isolated CECs from wild-type (WT) mice raised in SPF and GF conditions in Figure 3*A* were analyzed by means of an unpaired *t* test. Epithelial $H_2O_2$ release was reduced in WT GF CECs (*$P < .05$; n = 9–12 mice). (*B*) Freshly isolated CECs were assayed for the kinetic production of $H_2O_2$ in SPF-raised TLR4-KO and WT mice (n = 7–8 mice). (*C*) Functional production of $H_2O_2$ in TLR4-KO colonoids was verified by stimulating with interferon gamma (n = 3 cultures).

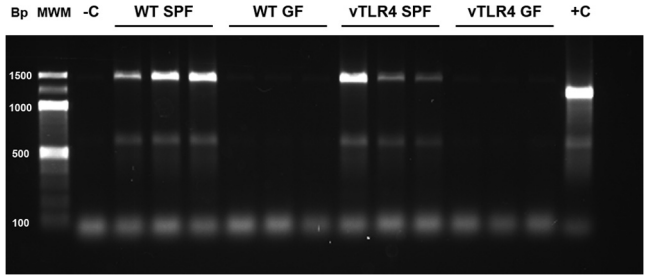


**Supplementary Figure 4.** 16s PCR of mouse stool after the CRC model. The presence of bacterial 16S ribosomal RNA was determined in the stool of SPF and GF villin-TLR4 and wild-type (WT) littermates to verify the GF status of mice at the end of the experiment. Each lane corresponds to 1 different mouse. Bp, base pair; –C, negative control (PCR run with water); +C, positive control (complementary DNA prepared from the stool of an SPF WT mouse); MWM, molecular weight marker.

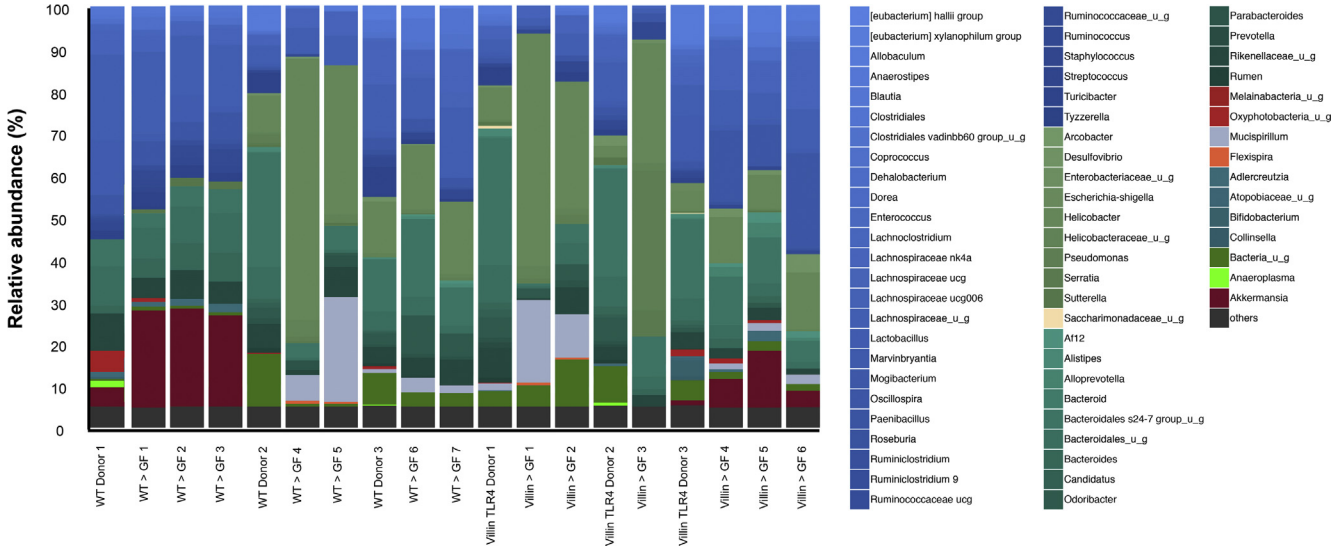


**Supplementary Figure 5.** 16s ribosomal RNA sequencing of mucosa-associated microbiota of donor and recipient mice. Wild-type GF recipient mice were engrafted with microbiota from C57Bl/6J or villin-TLR4 mice, and the mucosa of donor and recipient mice was sequenced to verify engraftment. Taxonomic distribution (genus level taxa) of the mucosa-associated microbiota from donor and recipient mice. Values represent the average relative abundance from each sample.

**Supplementary Table 1.** Quantitative Polymerase Chain Reaction Primers

| Gene | Sense | Primer | Reference |
|---|---|---|---|
| βActin | Forward | TGACAGGATGCAGAAGGAGA | e12 |
| | Reverse | CGCTCAGGAGGAGCAATG | |
| Duox2 | Forward | TCCAGAAGGCGCTGAACAG | NM_001362755.1 |
| | Reverse | GCGACCAAAGTGGGTGATG | |
| Duoxa2 | Forward | GCCTGGCTTTGCTCACCA | 21 |
| | Reverse | GAGGAGGAGGCTCAGGAT | |
| Gusβ | Forward | CCGATTATCCAGAGCGAGTATG | e13 |
| | Reverse | CTCAGCGGTGACTGGTTCG | |
| Nox1 | Forward | CTGACAAGTACTATTACACGAGAG | e14 |
| | Reverse | CATATATGCCACCAGCTTATGGAAG | |
| Noxa1 | Forward | TTCCTGATGACCACAACGCC | NM_172204.4 |
| | Reverse | CCGTAGTGCTCAGGACCCTC | |
| Noxo1 | Forward | ACTTAAACGCCTGTGCCATC | e15 |
| | Reverse | CCCCAACACTGCCCTAAGTA | |
| Cyba | Forward | TGTGGTGAAGCTTTTCGGGC | e15 |
| | Reverse | GGATGGCTGCCAGCAGATAGAT | |

**Supplementary Table 2.** Engraftment Percentages

| Taxonomic level | WT engraftment, % | Villin TLR4 engraftment, % |
|---|---|---|
| Phylum | 91.41 ± 8.35 | 85.17 ± 3.13 |
| Class | 93.15 ± 7.58 | 79.73 ± 9.98 |
| Genus | 88.76 ± 4.52 | 70 ± 12.77 |

WT, wild-type.